Capacitively coupled Josephson-junction chains: straight versus slanted coupling

2000 J. Phys.: Condens. Matter 12 943

(http://iopscience.iop.org/0953-8984/12/6/316)

J. Phys.: Condens. Matter **12** (2000) 943–957. Printed in the UK PII: S0953-8984(00)06477-8

Capacitively coupled Josephson-junction chains: straight versus slanted coupling

Mahn-Soo Choi†§, M Y Choi† and Sung-Ik Lee‡

† Department of Physics and Centre for Theoretical Physics, Seoul National University, Seoul 151-742, Korea

‡ Department of Physics and National Creative Research Initiative Centre for Superconductivity, Pohang University of Science and Technology, Pohang 790-784, Korea

Received 30 July 1999

Abstract. We investigate analytically the quantum phase transition in a system of two chains of ultrasmall Josephson junctions, coupled capacitively with each other. Two different schemes of the coupling, straight and slanted, between the two chains are considered. In both coupling schemes, as the coupling capacitance is increased, the transport of particle–hole pairs is found to drive a quantum phase transition of the Berezinskii–Kosterlitz–Thouless type from insulator to superconductor. A substantial discrepancy between the transition points in the two coupling schemes is observed, which reflects the difference between the transport mechanisms.

1. Introduction

Systems of ultrasmall tunnel junctions composed of metallic or superconducting electrodes have attracted considerable interest, owing to the remarkable roles of the Coulomb interaction. Of particular interest here is the Coulomb-blockade effect due to sufficiently large charging energy, which leads to single-charge (electron or Cooper-pair) tunnelling [1]. In order for this tunnelling to occur, however, it should be energetically favourable with respect to the electrostatic energy of the system. Otherwise, more complex elementary processes which involve several charge-tunnelling events should become dominant. For example, recent theoretical prediction [2] and experimental demonstration [3] have revealed the *cotunnelling* of electron–hole pairs in two one-dimensional (1D) arrays of metallic tunnel junctions coupled by large inter-array capacitances (see figure 1). Such cotunnelling of electron–hole pairs results in the interesting effect of current drag: the current fed through either of the chains induces a secondary current in the other chain. The primary and the secondary currents are comparable in magnitude, but opposite in direction.

A similar current-drag effect has also been observed in a system with a slightly different configuration, where each electrode in one array is coupled aslant to two adjacent electrodes in the other array (slanted coupling; see figure 2) [4]. Unlike in the case of straight coupling mentioned above (see figure 1), where the low-energy state can be preserved only if an electron and a hole tunnel simultaneously (cotunnelling), in this case of slanted coupling the low-energy state can be preserved for sequential tunnelling of an electron and a hole. It has been suggested that this correlated sequential tunnelling might be more favourable than the second-order process of cotunnelling via a quantum-mechanical virtual state.

§ Present address: Department of Physics and Astronomy, University of Basel, 4056 Basel, Switzerland.

0953-8984/00/060943+15$30.00

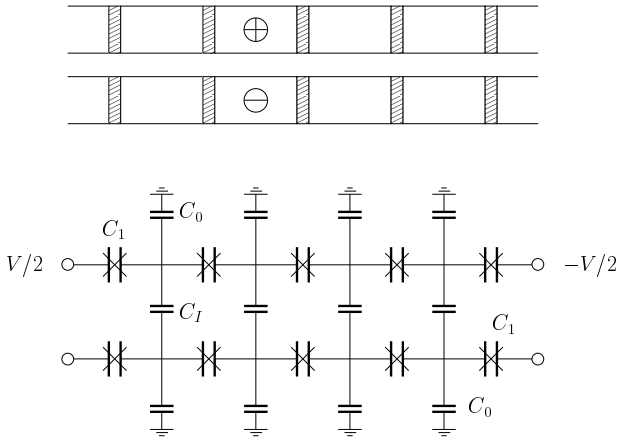

Figure 1. A schematic diagram and an equivalent circuit for the system with straight inter-chain coupling. Crosses superimposed on capacitor signs denote Josephson junctions, each with the coupling energy E_J and the junction capacitance C_1. The self-capacitance and the inter-chain capacitance are given by C_0 and C_I, respectively. After reference [2].

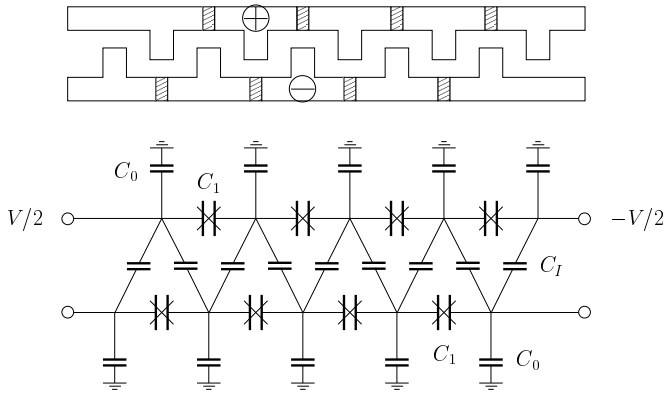

Figure 2. A schematic diagram and an equivalent circuit for the system with slanted inter-chain coupling. The symbols have the same meaning as those in figure 1. After reference [4].

More interestingly, in the case where the tunnelling junctions are composed of ultrasmall superconducting grains, the role of the electron–hole pair is played by the counterpart, the pair of an excess and a deficit in Cooper pairs, which we simply call a particle–hole pair. Furthermore, in such ultrasmall Josephson-junction systems, the competition between the charging energy and the Josephson coupling energy is well known to bring about the noble effects of quantum fluctuations [5–8]. It has recently been proposed that, combined with these quantum-fluctuation effects, the cotunnelling of particle–hole pairs in a capacitively coupled 1D Josephson-junction array (JJA) drives the quantum phase transition from insulator to superconductor [9]. Here, capacitive coupling should be distinguished from Josephson coupling (which allows inter-array Cooper-pair tunnelling). The quantum-fluctuation effects in the corresponding Josephson ladders have been studied in the literature [12].

In this paper, we extend the previous work [9] on two capacitively coupled 1D JJAs to consider both straight coupling and slanted coupling. The focus will be on the similarities of and differences between the two coupling schemes. It is shown that *in spite of the remarkable*

difference in the transport at the mesoscopic scale, the two cases are indistinguishable on long-time and large-length scales: as the coupling capacitance is increased, both cases exhibit the insulator-to-superconductor transition of the Berezinskii–Kosterlitz–Thouless (BKT) type [10, 11], whose superfluid phase is uniquely characterized by the condensation of particle–hole pairs and by perfect drag of supercurrents along the two chains. As contrasted with the cotunnelling process in the straight-coupling scheme, however, the correlated tunnelling nature of the elementary process in the slanted-coupling scheme results in a substantially lower transition point.

This paper is organized as follows. In section 2 we present the models for the systems with straight or slanted coupling, together with the regions of interest in the parameter space. Section 3 is devoted to the transformation of the models into equivalent two-dimensional (2D) systems of classical vortices, while section 4 examines the conductivity of the system in the vortex representation. On the basis of the results of sections 3 and 4, the phase transition and the current-drag effect are discussed in section 5, which constitutes the main part of this paper. In particular, a thorough discussion on the role of particle–hole pairs in the quantum phase transition and in the transport behaviour is given. Finally, section 6 concludes the paper.

2. Coupled chains of Josephson junctions

We consider a system of two coupled chains of Josephson junctions, where each chain is characterized by the Josephson coupling energy E_J and the charging energies $E_0 \equiv e^2/2C_0$ and $E_1 \equiv e^2/2C_1$ associated with the self-capacitance C_0 and the junction capacitance C_1, respectively (see figures 1 and 2). The two chains are coupled with each other by the capacitance C_I, with which the electrostatic energy $E_I \equiv e^2/2C_I$ is associated. Two different ways of coupling are considered: each island in one array is coupled either parallel to one island (straight coupling; figure 1) or aslant to two islands (slanted coupling; figure 2) in the other array. There is no Cooper-pair tunnelling allowed between the chains. The intra-chain capacitances are assumed to be so small ($E_0, E_1 \gg E_J$) that, without the coupling, the two chains would each be in the insulating phase separately [6]. It is further assumed that the coupling capacitance is sufficiently large compared with the intra-chain capacitances: $C_I \gg C_0, C_1$. In that case, the electrostatic energy of a particle–hole pair, which is of the order of E_I, is much smaller than that of an unpaired charge, which has the order of E_0 or E_1. For the most part, this work is devoted to the case of identical chains, but non-identical chains will also be briefly discussed.

The system with straight coupling is well described by the Hamiltonian $H = H_C + H_J$ with the Josephson-energy part

$$H_J = -E_J \sum_{\ell,x} \cos[\phi(\ell; x) - \phi(\ell; x+1)] \tag{1}$$

and the charging-energy part

$$H_C = 2E_I \sum_{\ell,\ell';x,x'} n(\ell; x)\mathbb{C}^{-1}_{\ell\ell'}(x, x')n(\ell'; x') \tag{2}$$

where the number $n(\ell; x)$ of excess Cooper pairs and the phase $\phi(\ell; x)$ of the superconducting order parameter in the grain at x on chain ℓ $(=1, 2)$ are quantum-mechanically conjugate variables: $[n(\ell; x), \phi(\ell'; x')] = \mathrm{i}\delta_{xx'}\delta_{\ell\ell'}$. Rescaling the capacitances in units of $2C_I$ (i.e., $C_0/2C_I \to C_0 \ll 1$ and $C_1/2C_I \to C_1 \ll 1$), we obtain the Fourier transform of the capacitance matrix given by equation (2) in the following form:

$$\widetilde{\mathbb{C}}(q) = \widetilde{C}(q)\begin{bmatrix} 1 & 0 \\ 0 & 1 \end{bmatrix} + \frac{1}{2}\begin{bmatrix} 1 & -1 \\ -1 & 1 \end{bmatrix} \tag{3}$$

where $\widetilde{C}(q) \equiv C_0 + C_1\Delta(q)$ with $\Delta(q) \equiv 2(1-\cos q)$ is the Fourier transform of the submatrix $C(x,x')$ within one chain. It is of interest to rewrite the charging-energy part as the sum $H_C = H_C^+ + H_C^-$, with each component given by

$$H_C^{\pm} = E_I \sum_{x,x'} n^{\pm}(x) V^{\pm}(x,x') n^{\pm}(x') \tag{4}$$

where $n^{\pm}(x) \equiv n(1;x) \pm n(2;x)$ and the interactions $V^{\pm}$ are given by their Fourier transforms

$$\widetilde{V}^{+}(q) = \frac{1}{\widetilde{C}(q)} \qquad \widetilde{V}^{-}(q) = \frac{1}{1+\widetilde{C}(q)}. \tag{5}$$

Since $\widetilde{C}(q) \ll 1$, we have $V^+ \gg V^-$ and it is obvious from equation (4) that the charge configurations which do not satisfy the condition $n^+(x) = 1$ for all x cost huge excitation energies of the order of E_0 or E_1. Accordingly, we expect the low-energy properties of the system to be dominated by the charge configurations with $n^+(x) = 0$ and $n^-(x) = 0, \pm 2$; in this case, $n_-(x)/2$ can be regarded as the number of particle–hole pairs located at x.

In the case of slanted coupling, the Josephson-energy part is still given by equation (1), but for the charging energy it is convenient to rescale the capacitances by $4C_I$. The dimensionless capacitance matrix then reads

$$\widetilde{\mathbb{C}}(q) = \widetilde{C}(q)\begin{bmatrix} 1 & 0 \\ 0 & 1 \end{bmatrix} + \frac{1}{4}\begin{bmatrix} 1 & -1 \\ -1 & 1 \end{bmatrix} + \frac{1}{4}\begin{bmatrix} 1 & -\mathrm{e}^{+\mathrm{i}q} \\ -\mathrm{e}^{-\mathrm{i}q} & 1 \end{bmatrix} \tag{6}$$

and the Hamiltonian of the system is given by

$$H_C = E_I \sum_{\ell,\ell';x,x'} n(\ell;x)\mathbb{C}^{-1}_{\ell\ell'}(x,x')n(\ell';x'). \tag{7}$$

With the peculiar form of the capacitance matrix in equation (6), the charging-energy part H_C in equation (7) can be decomposed into two components:

$$H_C^{\pm} = E_I \sum_{x,x'} n^{\pm}(x)V^{\pm}(x,x')n^{\pm}(x') + E_I \sum_{x,x'} n^{\pm}_{sl}(x)V^{\pm}(x,x')n^{\pm}_{sl}(x') \tag{8}$$

where $n^{\pm}_{sl}(x) \equiv n(1;x) \pm n(2;x-1)$ are defined aslant with respect to $n^{\pm}(x)$, and the interactions $V^{\pm}$ are again defined by the Fourier transforms:

$$\begin{aligned} \widetilde{V}^{+}(q) &= \frac{1+\widetilde{C}(q)}{4\widetilde{C}(q)[1+\widetilde{C}(q)] + \sin^2(q/2)} \\ \widetilde{V}^{-}(q) &= \frac{\widetilde{C}(q)}{4\widetilde{C}(q)[1+\widetilde{C}(q)] + \sin^2(q/2)}. \end{aligned} \tag{9}$$

As in the straight-coupling case, we have $V^+ \gg V^-$ from equation (9), and expect the particle–hole pairs ($n^-(x)/2$ or $n^-_{sl}(x)/2$) to play major roles in the transport. Unlike equation (5) for the straight-coupling case, however, equation (9) shows that the interaction V^- can be long ranged in general. For example, in the self-charging model ($C_1 = 0$), the interaction V^- between the particle–hole pairs ranges over the length scale $\lambda_* \equiv [16C_0(1+C_0)]^{-1}$, which is far larger than unity. This fact may have a significant effect in a system of finite size (see below). On the other hand, it is of interest that the nearest-neighbour charging model ($C_0 = 0$), which gives an infinitely long-range interaction in the case of a single (decoupled) chain, leads to V^- which is extremely short ranged (essentially on-site) in the system of coupled chains.

3. 2D classical-vortex representations

In this section, the two models, one described by equations (1) and (2) and the other by equations (1) and (7), are transformed into equivalent 2D classical systems of vortices. The resulting systems reveal clearly the nature of the phase transitions, which will be discussed in section 5.

3.1. Straight coupling

It is convenient to write the partition function of the system in the imaginary-time path-integral representation:

$$Z = \prod_{\ell,x,\tau} \sum_{n(\ell;x,\tau)} \int_0^{2\pi} \mathrm{d}\phi(\ell;x,\tau)\ \exp[-\mathcal{S}] \tag{10}$$

with the Euclidean action

$$\mathcal{S} = \frac{1}{2\sqrt{2}K} \sum_{\ell,\ell'} \sum_{x,x',\tau} n(\ell;x,\tau)\mathbb{C}^{-1}_{\ell\ell'}(x,x')n(\ell;x',\tau) - \sqrt{2}K \sum_{\ell} \sum_{x,\tau} \cos \nabla_x \phi(\ell;x,\tau) + \mathrm{i} \sum_{\ell} \sum_{x} n(\ell;x,\tau)\, \nabla_\tau \phi(\ell;x,\tau) \tag{11}$$

where the coupling constant has been defined to be $K \equiv \sqrt{E_J/8E_I}$, and ∇_x and ∇_τ denote the difference operators with respect to x and τ, respectively. The time has been rescaled by the Josephson-plasma frequency $\omega_p \equiv \sqrt{4E_I E_J}/\hbar$, and the (imaginary-) time slice $\delta\tau$ has been chosen to be unity (in units of $1/\omega_p$) [13]. The highly symmetric form of equation (11) with respect to space and (imaginary) time makes it useful to introduce the space-time 2-vector notation $\boldsymbol{r} \equiv (x,\tau)$ and analogous notation for all other vector variables. We then employ the Villain approximation [14] to rewrite the cosine term as the summation over an integer field $\{m_x(\ell;\boldsymbol{r})\}$. Furthermore, with the aid of the Poisson resummation formula [14] and Gaussian integration, we express the charging-energy term as the summation over another integer field $\{m_\tau(\ell;\boldsymbol{r})\}$ and obtain the partition function

$$Z \sim \prod_{\ell;\boldsymbol{r}} \sum_{\boldsymbol{m}(\ell;\boldsymbol{r})} \int_{-\infty}^{\infty} \mathrm{d}\phi(\ell;\boldsymbol{r})\ \exp\{-\mathcal{S}\} \tag{12}$$

with

$$\mathcal{S} = \frac{K}{\sqrt{2}} \sum_{\ell,\ell';\boldsymbol{r},\boldsymbol{r}'} \mathbb{C}_{\ell\ell'}(x,x')\delta_{\tau\tau'}[\nabla_\tau\phi(\ell;\boldsymbol{r}) - 2\pi m_\tau(\ell;\boldsymbol{r})][\nabla_\tau\phi(\ell';\boldsymbol{r}') - 2\pi m_\tau(\ell';\boldsymbol{r}')] + \frac{K}{\sqrt{2}} \sum_{\ell;\boldsymbol{r}} [\nabla_x\phi(\ell;\boldsymbol{r}) - 2\pi m_x(\ell;\boldsymbol{r})]^2 . \tag{13}$$

Using the variables $\phi^{\pm}(\boldsymbol{r}) \equiv \phi(1;\boldsymbol{r}) \pm \phi(2;\boldsymbol{r})$ and $\boldsymbol{m}^{\pm}(\boldsymbol{r}) \equiv \boldsymbol{m}(1;\boldsymbol{r}) \pm \boldsymbol{m}(2;\boldsymbol{r})$ in the place of $\phi(\ell;\boldsymbol{r})$ and $\boldsymbol{m}(\ell;\boldsymbol{r})$, respectively, we decompose the Euclidean action in equation (13) into two parts: $\mathcal{S} = \mathcal{S}^+ + \mathcal{S}^-$, with

$$\mathcal{S}^{\pm} \equiv \frac{K}{2\sqrt{2}} \sum_{\boldsymbol{r},\boldsymbol{r}'} C^{\pm}(x,x')\delta_{\tau\tau'}[\nabla_\tau\phi^{\pm}(\boldsymbol{r}) - 2\pi m^{\pm}_\tau(\boldsymbol{r})][\nabla_\tau\phi^{\pm}(\boldsymbol{r}') - 2\pi m^{\pm}_\tau(\boldsymbol{r}')] + \frac{K}{2\sqrt{2}} \sum_{\boldsymbol{r}} [\nabla_x\phi^{\pm}(\boldsymbol{r}) - 2\pi m^{\pm}_x(\boldsymbol{r})]^2 \tag{14}$$

where the new capacitance matrices $C^{\pm}(x,x')$ have been defined according to $\widetilde{C}^{+}(q) \equiv \widetilde{C}(q)$ and $\widetilde{C}^{-}(q) \equiv 1 + \widetilde{C}(q)$. One now follows the standard procedure [6, 15] to integrate out

$\{\phi^{\pm}(\boldsymbol{r})\}$ and obtains, apart from the irrelevant spin-wave part, the desired 2D system of classical vortices, which is also decomposed into the two subsystems. It is described by the Hamiltonian $H_V = H_V^+ + H_V^-$ with

$$H_V^{\pm} \equiv \sqrt{2}\pi^2 K \sum_{\boldsymbol{r},\boldsymbol{r}'} v^{\pm}(\boldsymbol{r}) U^{\pm}(\boldsymbol{r}-\boldsymbol{r}') v^{\pm}(\boldsymbol{r}') \tag{15}$$

where the vortices $v^{\pm}(\boldsymbol{r})$ are related to the vortices $v(\ell;\boldsymbol{r})$ on chain ℓ via

$$v^{\pm}(\boldsymbol{r}) \equiv v(1;\boldsymbol{r}) \pm v(2;\boldsymbol{r})$$

and the interactions between vortices are defined via their Fourier transforms:

$$\widetilde{U}^{\pm}(\boldsymbol{q}) = \frac{\widetilde{C}^{\pm}(q)}{\Delta(q) + \widetilde{C}^{\pm}(q)\,\Delta(\omega)}. \tag{16}$$

It is instructive to notice that the vortices $v^{\pm}$ represent some sort of correlations between the two chains in the system. In figure 3 a configuration of two vortices, $v(1;\boldsymbol{r}) = +1$ and $v(2;\boldsymbol{r}') = +1$ $(\boldsymbol{r} \neq \boldsymbol{r}')$, is represented. This configuration corresponds to a pair composed of the vortex $v^-(\boldsymbol{r}) = +1$ and the antivortex $v^-(\boldsymbol{r}') = -1$, which tend to be bound to each other; at the same time, it also gives two vortices $v^+(\boldsymbol{r}) = v^+(\boldsymbol{r}') = +1$, which are inclined to repel each other. We thus have opposite tendencies for v^+ and v^-, in the configuration consisting of a vortex on one space-time layer and an antivortex on the other. As shown in section 5, it is the vortices $\{v^-\}$ that provide a manifestation of the particle–hole pairs and play a major role in the quantum phase transition.

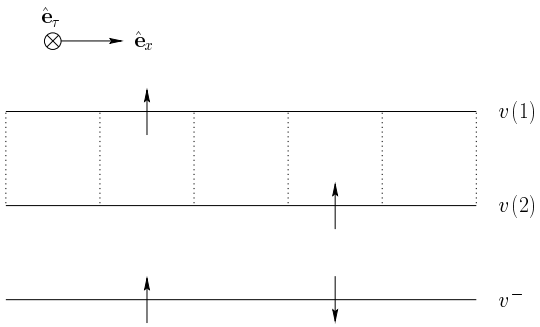

Figure 3. The displacement vortex v^-. The configuration of one vortex $v(1;\boldsymbol{r}) = +1$ on space-time layer 1 and another $v(2;\boldsymbol{r}') = +1$ on layer 2 $(\boldsymbol{r} \neq \boldsymbol{r}')$ corresponds to a pair composed of a displacement vortex $v^-(\boldsymbol{r}) = +1$ and antivortex $v^-(\boldsymbol{r}') = -1$.

Equation (16) shows that $U^-(0)$ is always divergent, thus giving rise to the *vortex number equality condition* $\sum_r v(1;\boldsymbol{r}) = \sum_r v(2;\boldsymbol{r})$ or, equivalently, the vorticity neutrality condition $\sum_r v^-(\boldsymbol{r}) = 0$ for v^- in equation (15). A similar neutrality condition, $\sum_r v^+(\boldsymbol{r}) = 0$, should be satisfied unless $C_0 = 0$ (see reference [8]). It is important here to notice that the two fields v^+ and v^- are in fact not independent of each other since $m_\mu(\ell;\boldsymbol{r})$ in equation (13) and hence $v(\ell;\boldsymbol{r})$ can take only integer values. As depicted with open circles in figure 4, (v^+, v^-) at each $\boldsymbol{r}$ can take the form of only half of the elements in the product set of integers $\mathbb{Z} \times \mathbb{Z}$; v^+ and v^- are *topologically coupled* with each other. However, this topological coupling turns out to be irrelevant and can be safely neglected, as discussed in section 5.

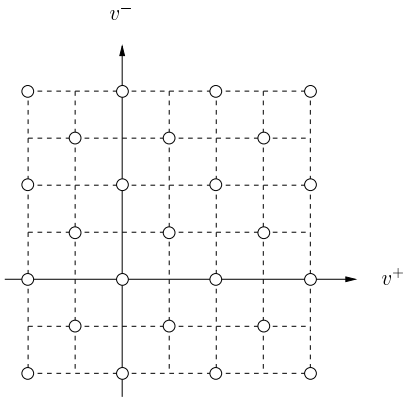

Figure 4. Topological coupling of v^+ and v^-. At each space-time position, (v^+, v^-) can take the form of only half of the elements in $\mathbb{Z} \times \mathbb{Z}$, as depicted with the open circles.

3.2. Slanted coupling

In the same way as that leading to equation (13) from the path-integral representation of the partition function (equation (10)), one can obtain the partition function for slanted coupling:

$$Z \sim \prod_{\ell;\boldsymbol{r}} \sum_{\boldsymbol{m}(\ell;\boldsymbol{r})} \int_{-\infty}^{\infty} \mathrm{d}\phi(\ell;\boldsymbol{r}) \ \exp\{-\mathcal{S}\} \tag{17}$$

with the Euclidean action

$$\begin{aligned}\mathcal{S} = K \sum_{\ell,\ell';\boldsymbol{r},\boldsymbol{r}'} \mathbb{C}_{\ell\ell'}(x,x')\delta_{\tau\tau'}[\nabla_\tau\phi(\ell;\boldsymbol{r}) - 2\pi m_\tau(\ell;\boldsymbol{r})][\nabla_\tau\phi(\ell';\boldsymbol{r}') - 2\pi m_\tau(\ell';\boldsymbol{r}')] \\ + K \sum_{\ell;\boldsymbol{r}} [\nabla_x\phi(\ell;\boldsymbol{r}) - 2\pi m_x(\ell;\boldsymbol{r})]^2\end{aligned} \tag{18}$$

where the time has been rescaled by the corresponding Josephson-plasma frequency $\omega_p \equiv \sqrt{2E_I E_J}/\hbar$. Unlike the previous straight-coupling case, the last term in the capacitance matrix $\mathbb{C}$ in equation (6) makes it useless to replace the variables $\phi(\ell;\boldsymbol{r})$ and $\boldsymbol{m}(\ell;\boldsymbol{r})$ by $\phi^{\pm}(\boldsymbol{r})$ and $\boldsymbol{m}^{\pm}(\boldsymbol{r})$, respectively. Instead, we thus integrate out $\phi(\ell;\boldsymbol{r})$ directly to get the Hamiltonian for 2D classical vortices:

$$\begin{aligned}H_V = 4\pi^2 K \sum_{\ell;\boldsymbol{r},\boldsymbol{r}'} v(\ell;\boldsymbol{r})U_0(\boldsymbol{r}-\boldsymbol{r}')v(\ell;\boldsymbol{r}') + 4\pi^2 K \sum_{\boldsymbol{r},\boldsymbol{r}'} v^-(\boldsymbol{r})U_I(\boldsymbol{r}-\boldsymbol{r}')v^-(\boldsymbol{r}') \\ + 4\pi^2 K \sum_{\boldsymbol{r},\boldsymbol{r}'} v^-_{sl}(\boldsymbol{r})U_I(\boldsymbol{r}-\boldsymbol{r}')v^-_{sl}(\boldsymbol{r}')\end{aligned} \tag{19}$$

where the vortex interactions are again given by the Fourier transforms

$$\begin{aligned}\widetilde{U}_0(\boldsymbol{q}) &= \frac{\widetilde{C}(q)}{T(\boldsymbol{q})}\left\{\Delta(q) + \left[1+\widetilde{C}(q)\right]\Delta(\omega)\right\} + \frac{\Delta(q)\Delta(\omega)}{16T(\boldsymbol{q})} \\ \widetilde{U}_I(\boldsymbol{q}) &= \frac{\Delta(q)}{4T(\boldsymbol{q})}\end{aligned} \tag{20}$$

with

$$T(\boldsymbol{q}) = \left[\Delta(q) + \widetilde{C}(q)\Delta(\omega)\right]\left\{\Delta(q) + \left[1+\widetilde{C}(q)\right]\Delta(\omega)\right\} + \frac{1}{16}\Delta(q)\Delta^2(\omega). \tag{21}$$

In equation (19), the vortices v^- and v_{sl}^- are defined by the direct difference $v^-(\boldsymbol{r}) \equiv [v(1;\boldsymbol{r}) - v(2;\boldsymbol{r})]$ and by the slanted difference $v_{sl}^-(\boldsymbol{r}) \equiv [v(1;\boldsymbol{r}) - v(2;\boldsymbol{r}+\hat{e}_x)]$, respectively (see figure 5).

Here the appearance of the additional term depending on v_{sl}^- is not surprising since a vortex on one space-time layer leads to two alternative (nearest-neighbouring) sites for the corresponding vortex on the other space-time layer. However, at the long-time and large-length scales in which we are interested, any configuration of v_{sl}^- gives the same energy as the corresponding configuration of v^-, as can be observed in figure 5. Thus, v_{sl}^- in the last term in equation (19) can be simply replaced by v^-, leading to

$$H_V \simeq 4\pi^2 K \sum_{\ell;\boldsymbol{r},\boldsymbol{r}'} v(\ell;\boldsymbol{r}) U_0(\boldsymbol{r}-\boldsymbol{r}') v(\ell;\boldsymbol{r}') + 8\pi^2 K \sum_{\boldsymbol{r},\boldsymbol{r}'} v^-(\boldsymbol{r}) U_I(\boldsymbol{r}-\boldsymbol{r}') v^-(\boldsymbol{r}'). \tag{22}$$

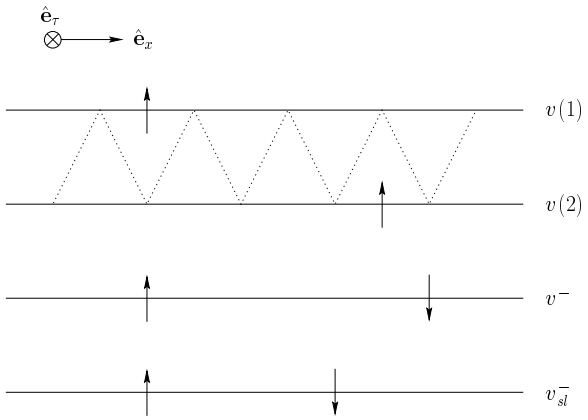

Figure 5. The displacement vortex for slanted coupling. At large (space-time) lengths, the vortex–antivortex pair of v_{sl}^- yields the same energy as that of v^-.

This point can also be shown in a more rigorous way by rewriting the Hamiltonian in equation (19) in terms of $v^\pm(\boldsymbol{r})$: $H_V = H_V^+ + H_V^- + \delta H_V$, where $H_V^\pm$ has the anticipated form

$$H_V^\pm = 2\pi^2 K \sum_{\boldsymbol{r},\boldsymbol{r}'} v^\pm(\boldsymbol{r}) U^\pm(\boldsymbol{r}-\boldsymbol{r}') v^\pm(\boldsymbol{r}') \tag{23}$$

with the vortex interactions

$$\begin{aligned} \widetilde{U}^+(\boldsymbol{q}) &= \widetilde{U}_0(\boldsymbol{q}) \\ \widetilde{U}^-(\boldsymbol{q}) &= \frac{1+\widetilde{C}(q)}{T(\boldsymbol{q})}\left[\Delta(q) + \widetilde{C}(q)\Delta(\omega)\right] + \frac{\Delta(q)\Delta(\omega)}{16T(\boldsymbol{q})}. \end{aligned} \tag{24}$$

The term δH_V, defined to be

$$\delta H_V = \frac{\pi^2}{4} K \sum_{\alpha,\beta=\pm} \sum_{\boldsymbol{r},\boldsymbol{r}'} v^\alpha(\boldsymbol{r})\, \delta U^{\alpha\beta}\, v^\beta(\boldsymbol{r}') \tag{25}$$

with

$$\delta\tilde{U}^{\alpha\beta}(\boldsymbol{q}) = \frac{\Delta(q)}{T(\boldsymbol{q})} \begin{bmatrix} +\Delta(q) & +2\mathrm{i}\sin q \\ -2\mathrm{i}\sin q & -\Delta(q) \end{bmatrix} \tag{26}$$

describes the interaction between v^+ and v^-. Since the numerator in the interaction $\delta\widetilde{U}^{\alpha\beta}(\boldsymbol{q})$ is of third order in $\boldsymbol{q}$, at long times and large lengths ($\boldsymbol{q} \to 0$), δH_V can be ignored compared

with $H_V^{\pm}$. Moreover, in the low-frequency and low-momentum limit (i.e. $q^2 \ll \lambda_*^{-1} \equiv 16C_0(1 + C_0)$ and $\omega^2 \ll 1$ for the self-charging model ($C_1 = 0$), and $q^2, \omega^2 \ll 1$ for the nearest-neighbour charging model ($C_0 = 0$)), the vortex interactions in equation (24) simply reduce to those for straight coupling, given by equation (16). For this reason, it is concluded that at long times and large lengths, the 2D vortex representations for straight and slanted couplings are equivalent to each other except for the different coupling constants: $K/\sqrt{2}$ for straight coupling and K for slanted coupling. Here it should be pointed out that the emergence of the momentum scale λ_*^{-1} for the self-charging model traces back to the long-range interaction between the particle–hole pairs in equation (9). As a result, in a system of finite size, the interaction U^- between the vortices v^- may be anisotropic in the space and time directions.

4. Generalized conductivity

The mathematical mapping in the previous section allows us to study the existence and the universality class of the phase transition. It is further needed to identify the phases on both sides of the transition (see section 5); for this purpose, it is convenient to examine the responses of the system to external perturbations. In this section, we consider the generalized conductivity, i.e., the current response function $\sigma_{\ell\ell'}(\omega)$ of chain ℓ to the voltage applied along chain ℓ' (see figure 1 and figure 2), expressing it in terms of the vortex representation discussed in the previous section.

The standard linear response theory gives the generalized conductivity in the form of the analytic continuation

$$\sigma_{\ell\ell'}(\omega) = \frac{1}{\mathrm{i}\omega} \lim_{q\to 0} \widetilde{\mathcal{G}}_{\ell\ell'}(q, \mathrm{i}\omega' \to \omega + \mathrm{i}0^+) \tag{27}$$

where $\widetilde{\mathcal{G}}_{\ell\ell'}$ is the Fourier transform of the imaginary-time Green's function

$$\mathcal{G}_{\ell\ell'}(x, \tau) = \left\langle T_\tau [I(\ell; x, \tau) I(\ell'; 0, 0)] \right\rangle \tag{28}$$

with the time-ordered product T_τ and the current operator $I(\ell; x) \equiv \sin \nabla_x \phi(\ell; x)$. Owing to the symmetry between the two chains, the components σ_{11} and σ_{21} can be written as

$$\sigma_{11}(\omega) = \frac{1}{4}\left[\sigma_+(\omega) + \sigma_-(\omega)\right] \tag{29}$$

$$\sigma_{21}(\omega) = \frac{1}{4}\left[\sigma_+(\omega) - \sigma_-(\omega)\right] \tag{30}$$

where the $\sigma_\pm$ have been defined in a manner analogous to equations (27) and (28), with $I^{\pm}(x) \equiv I(1; x) \pm I(2; x)$. In the same manner as in section 3, one can get the vortex representation of the corresponding Green's functions $\mathcal{G}_\pm$ (see the appendix):

$$\mathcal{G}_\pm(\boldsymbol{r}_1, \boldsymbol{r}_2) = \nabla_{\tau_1}\nabla_{\tau_2}\left[-\frac{\gamma}{K}U^{\pm}(\boldsymbol{r}_1, \boldsymbol{r}_2) + 4\pi^2 \sum_{\boldsymbol{r}_1', \boldsymbol{r}_2'} U^{\pm}(\boldsymbol{r}_1, \boldsymbol{r}_1') U^{\pm}(\boldsymbol{r}_2, \boldsymbol{r}_2') \left\langle v^{\pm}(\boldsymbol{r}_1') v^{\pm}(\boldsymbol{r}_2') \right\rangle_V\right] \tag{31}$$

where $\gamma = \sqrt{2}/1$ for straight/slanted coupling, and the average $\langle \cdots \rangle_V$ is taken with respect to the total vortex Hamiltonian $H_V = H_V^+ + H_V^-$. In equation (31), the Hamiltonians $H_V^{\pm}$ in equation (15) and the interactions $U^{\pm}$ in equation (16) have been used for both straight and slanted couplings, which should be valid at long times and large lengths. One advantage of the representation in equation (31) is that the vortex contribution in the second term can be estimated by means of the standard renormalization group (RG) approach for 2D classical vortices [5, 11, 14].

5. Quantum phase transitions

In this section, we turn to the main subjects of this work and investigate the quantum phase transitions and current-drag effects in the system, based on the 2D classical-vortex representations given by equations (15) and (23) together with the response functions in equation (27). In section 2, it has been established that, aside from the difference in the coupling constant, the two coupling schemes are equivalent at long times and large lengths. We thus focus on the straight-coupling case; the results are also applicable in full to the slanted-coupling case with the coupling constant properly adjusted. Some notable differences between the two cases will be discussed at the end of the section.

It is not difficult to understand the physics described by H_V^+ and by H_V^-, given by equation (15), separately. Unless $C_0 = 0$, the length-dependent anisotropy due to $\widetilde{C}^+(q) = \widetilde{C}(q)$ ($\ll 1$) in the interaction $\widetilde{U}^+(\boldsymbol{q})$ given by equation (16) fades out on (space-time) length scales larger than $\sqrt{C_1/C_0}$; thereby $\widehat{U}^+(\boldsymbol{r}) \equiv 2\pi[U^+(0) - U^+(\boldsymbol{r})]$ simply reduces to the isotropic logarithmic interaction

$$\widehat{U}^+(\boldsymbol{r}) \approx \sqrt{C_0}\ln r \tag{32}$$

for $r \gg 1$. This results in the usual vortex Hamiltonian

$$H_V^+ \approx -\pi K_{eff}^+ \sum_{\boldsymbol{r},\boldsymbol{r}'} v^+(\boldsymbol{r})\ln|\boldsymbol{r} - \boldsymbol{r}'|v^+(\boldsymbol{r}) \tag{33}$$

with the effective coupling constant $K_{eff}^+ \equiv \sqrt{E_J/16E_0}$. In the system with $E_0, E_1 \gg E_J$, which is considered here, K_{eff} is substantially smaller than the BKT transition point $K_{BKT} \approx 2/\pi$. Accordingly, the vortices v^+ always form a neutral plasma of free vortices regardless of K (i.e., regardless of C_I). In the case $C_0 = 0$, on the other hand, $U^+(\boldsymbol{r})$ becomes short ranged: $U^+(\boldsymbol{r}) \sim \sqrt{C_1}\exp(-r/\sqrt{C_1})$; still the vortices v^+ form a (non-neutral) plasma of free vortices. Thus in any case the system of vortices v^+ is concluded to form a plasma of free vortices, regardless of the value of K. We next examine the behaviour of the vortices v^- described by H_V^-. With the short-distance anisotropy neglected, we have $\widetilde{U}^-(\boldsymbol{q}) \approx 1/[\Delta(q) + \Delta(\omega)]$ and the interaction $\widehat{U}^-(\boldsymbol{r}) \equiv 2\pi[U^-(0) - U^-(\boldsymbol{r})]$ isotropic in the space and time directions and logarithmic in distance: $\widehat{U}(\boldsymbol{r}) \approx \log r$. This leads to the 2D Coulomb-gas Hamiltonian for v^-:

$$H_V^- \approx -\sqrt{2}\pi^2 K \sum_{\boldsymbol{r},\boldsymbol{r}'} v^-(\boldsymbol{r})\ln|\boldsymbol{r} - \boldsymbol{r}'|v^-(\boldsymbol{r}') \tag{34}$$

which indicates that the system of vortices v^- exhibits a BKT-type phase transition at $K = K_c^- \equiv \sqrt{2}K_{BKT} \approx 2\sqrt{2}/\pi$.

At this point, it appears suggestive to conclude that as K is decreased, the total system H_V undergoes a BKT-type transition at $\sqrt{2}K_{BKT}$ which is entirely driven by the vortices v^-, with v^+ playing no role. This scenario, however, should be carefully checked against the topological coupling between v^+ and v^- discussed in the previous section. To this end, it is convenient to consider the subsystem $\{v^*\}$ of $\{v^+\}$, satisfying $v^-(\boldsymbol{r}) = 0$ for all $\boldsymbol{r}$. In this subsystem, $v^*(\boldsymbol{r})$ can take only even values, and the Hamiltonian can be written in the form

$$H_V^* \approx -\pi(4K_{eff}^+)\sum_{\boldsymbol{r},\boldsymbol{r}'} \frac{v^*(\boldsymbol{r})}{2}\ln|\boldsymbol{r} - \boldsymbol{r}'|\frac{v^*(\boldsymbol{r}')}{2} \tag{35}$$

unless $C_0 = 0$. Under the assumption that $E_0, E_1 \gg E_J$, we again have $4K_{eff}^+ \ll K_{BKT}$, and there are a significant number of free vortices of v^*, which is obviously true also in the case $C_0 = 0$. These free vortices of v^* substantially affect the topological coupling and eventually make it irrelevant: as illustrated in figure 6, the vortex–antivortex pair of v^- is always accompanied by two vortices of v^+ (enclosed in dotted ellipses). The interaction between these

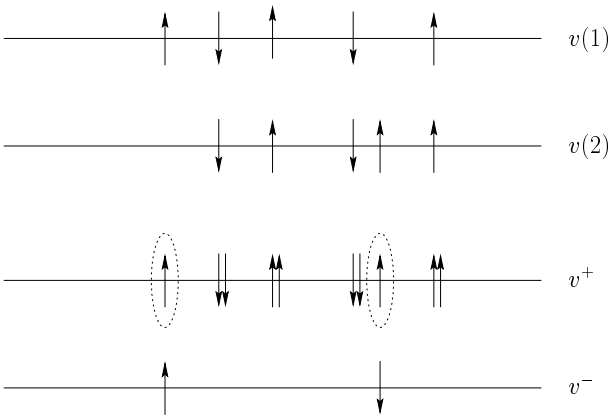

Figure 6. Due to the topological coupling, the vortex–antivortex pair of the displacement vortices v^- induces two vortices of v^+ (indicated by dotted ellipses). The interaction between these two vortices is, however, completely screened out by the free vortices of v^+ with vorticity ± 2 (represented by the double arrows).

two vortices of v^+ is completely screened out by the free vortices of v^* (represented by double arrows). The two vortices of v^+, therefore, do not affect the interaction energy of the vortex–antivortex pair of v^-, changing only slightly the fugacity of v^-. It is thus concluded that as K is increased, *the system does indeed exhibit a BKT-type transition at* $K_c^{st} \approx \sqrt{2}K_{BKT} \approx 2\sqrt{2}/\pi$, *which is exclusively attributable to the vortices* v^-.

To examine the states of the system on both sides of K_c^{st}, we first note that the vortices $v^{\pm}(\boldsymbol{r})$ are topological singularities in the 2D space-time configurations of the phases $\phi^{\pm}(\boldsymbol{r}) \equiv \phi(1;\boldsymbol{r}) \pm \phi(2;\boldsymbol{r})$. The plasma of free vortices of v^+ leads to complete disorder of ϕ^+. According to the uncertainly relation between ϕ^+ and the conjugate variable $n^+(x)/2$, i.e., $\Delta\phi^+ \, \Delta(n^+/2) \gtrsim 1$, this indicates that $n^+(x)$ for each x takes a well-defined value, which should be zero due to the large single-charge (Cooper-pair) excitation energy of the order of E_0 or of E_1. Due to this condition $n^+(x) = 0$, the variable $n^-(x)/2$ conjugate to ϕ^- measures precisely the number of pairs of an excess and a deficit in Cooper pairs (i.e., particle–hole pairs). Furthermore, it is also noted that the effective model in equation (15) or equation (34) is a vortex representation of the quantum phase model [5, 8]:

$$H_{QPM} = \frac{1}{\sqrt{2}K} \sum_x \left[\frac{n^-(x)}{2}\right]^2 + \frac{K}{\sqrt{2}} \sum_x \cos \nabla_x \phi^-(x). \tag{36}$$

Therefore, the BKT-type phase transition at K_c^{st} driven by v^- is nothing but an insulator-to-superfluid transition of the particle–hole pairs: although particle–hole pairs are always the lowest excitations, they cannot move along the system without an external bias below K_c^{st}, due to the Coulomb blockade associated with the charging energy E_I. For $K > K_c^{st}$, on the other hand, the particle–hole pairs condense to form a superfluid and can move freely along the system (see figure 7). The formation of bound dipoles of vortices v^- is an effective manifestation of the condensation of the particle–hole pairs.

Such particle–hole pair transport can be confirmed by examining the current responses of the two chains, given by equation (27). Due to the free vortices of v^+, it follows directly from equation (31) that $\sigma_+(\omega)$ vanishes (for $\omega \ll 1$). On the other hand, the tightly bound

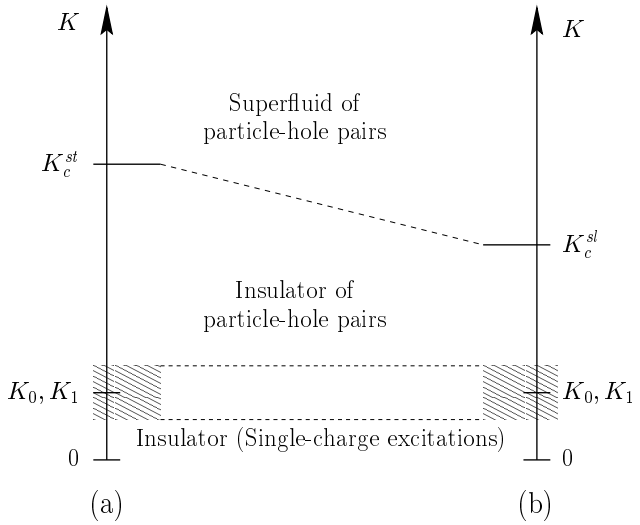

Figure 7. Schematic phase diagrams of capacitively coupled Josephson-junction chains (a) with straight coupling and (b) with slanted coupling. The intra-chain coupling constants K_0 and K_1 are defined by $K_0 \equiv \sqrt{E_J/8E_0} \propto \sqrt{C_0}$ and by $K_1 \equiv \sqrt{E_J/8E_1} \propto \sqrt{C_1}$, respectively. In the text, only the region of $K \gg K_0, K_1$, where particle–hole pairs are relevant, is considered. The shaded regions in the picture indicate the crossover from the regime with the single charges dominating to that with the particle–hole pairs dominating.

vortex–antivortex pairs of v^- above K_c^{st} result in the response function ($\omega \ll 1$)

$$\sigma_-(\omega) = \frac{2\pi}{\sqrt{2}K}\left(2 - \frac{K}{K_R}\right)\delta(\omega) \tag{37}$$

and

$$\sigma_{11}(\omega) = -\sigma_{21}(\omega) = \frac{\pi}{2\sqrt{2}K}\left(2 - \frac{K}{K_R}\right)\delta(\omega) \tag{38}$$

where the renormalized coupling constant K_R is defined according to

$$\frac{\sqrt{2}}{K_R} \equiv \frac{\sqrt{2}}{K} - \frac{\pi^2}{2}\sum_{\boldsymbol{r}} |\boldsymbol{r}|^2 \left\langle v^-(\boldsymbol{r}) v^-(\boldsymbol{0})\right\rangle. \tag{39}$$

The system thus exhibits *superconductivity* and carries currents along the two chains that are *equally large in magnitude but opposite in direction*. This perfect drag of supercurrents reveals that the charges do indeed transport in the form of particle–hole pairs, which are bound by the electrostatic energy E_I associated with C_I. For $K < K_c^{st}$, on the other hand, the system displays insulating particle–hole current–voltage characteristics, qualitatively the same as those in references [2–4].

The whole argument put forward so far in this section also holds for slanted coupling if one simply replaces $K/\sqrt{2}$ by K. Accordingly, the system with slanted coupling exhibits a BKT-type transition at $K_c^{sl} \approx K_{BKT}$, and the superfluid state is characterized by the response functions

$$\sigma_{11}(\omega) = -\sigma_{21}(\omega) = \frac{\pi}{4K}\left(2 - \frac{K}{K_R}\right)\delta(\omega) \tag{40}$$

where

$$\frac{1}{K_R} \equiv \frac{1}{K} - \frac{\pi^2}{2}\sum_{\boldsymbol{r}} |\boldsymbol{r}|^2 \left\langle v^-(\boldsymbol{r}) v^-(\boldsymbol{0})\right\rangle. \tag{41}$$

It is interesting, however, to notice that K_c^{sl} is far smaller than K_c^{st} (see figure 7). This reflects the difference between the two coupling schemes as regards the underlying transport mechanism: the correlated sequential tunnelling of particle–hole pairs, which is a first-order process, is more likely than the second-order cotunnelling process. It should also be pointed out that due to the additional length scale λ_* ($\gg 1$) (see the comments below equations (9) and (26)), the system size is required to be sufficiently large for the universal behaviour of the BKT transition.

6. Conclusions

We have investigated the properties associated with particle–hole pairs in two capacitively coupled Josephson-junction chains, considering both the system with straight coupling and that with slanted coupling. In particular, the transport of particle–hole pairs has been found to drive the BKT-type insulator-to-superfluid transition with the coupling capacitance varied, in both coupling schemes. The superfluid phase present in the regime of large coupling capacitance is uniquely characterized by the absolute drag of supercurrents along the two chains.

Such capacitively coupled Josephson-junction chains can presumably be realized in experiment, even by present techniques. Recent advances in micro-fabrication techniques have already made it possible to create large arrays of ultrasmall Josephson junctions [16]. Furthermore, the experimental realization of the capacitively coupled submicron metal-junction arrays [3, 4] illustrates that large inter-array capacitances can also be fabricated from two Josephson-junction arrays.

In view of such an experimental situation, it is desirable to examine the assumptions made in this work and to discuss possible generalizations to more realistic cases. First of all, note that this work has considered the chains mainly in the self-charging ($C_1 = 0$) or nearest-neighbour charging ($C_0 = 0$) limit. On the basis of reference [8], however, it can be argued that the qualitative results remain valid for realistic cases of general capacitances. The assumption of identical chains made throughout this paper can also be justified as follows: the difference in the intra-chain capacitances leads to additional coupling between the vortices v_μ^+ and v_μ^- with the coupling strength proportional to the difference. The arguments on identical chains therefore remain valid qualitatively as long as

$$|\widetilde{C}(1;\boldsymbol{q}) - \widetilde{C}(2;\boldsymbol{q})| \ll |\widetilde{C}(1;\boldsymbol{q}) + \widetilde{C}(2;\boldsymbol{q})|.$$

The difference in the Josephson coupling energy, on the other hand, can be effectively incorporated in the capacitance difference by renormalizing the parameters, since all the effects considered in this work depend only on the relative strength of the energy of the Josephson coupling to the charging energies.

We also point out that quasiparticles have been safely neglected in obtaining equilibrium properties at zero temperature. At finite temperatures or large voltage bias, there may exist a significant number of quasiparticles, which cause dissipation in the system [16]; still in the weak-dissipation limit, our results should not be affected qualitatively [7]. Furthermore, it should be kept in mind that too high a voltage or current biasing one chain can destroy the bound pairs of particles and holes, making the supercurrent in the other chain vanish.

Finally, we remark that it will be valuable to investigate the effects of charge frustration, induced by the gate voltage applied between the substrate and the array, in the slanted-coupling case. From the results of the previous work [9], it can be anticipated that the charge frustration should lead to a rich phase diagram, although the details remain to be accounted for more carefully.

Acknowledgments

This work was supported in part by the Korea Research Foundation and by the Korea Science and Engineering Foundation (MSC and MYC), as well as by the Korea Science and Engineering Foundation through the National Creative Research Initiative Programme (SIL).

Appendix

This appendix presents the derivation of the vortex representation of the imaginary-time Green's function given by equation (31). For simplicity, only $\mathcal{G}_-$ for straight coupling is derived here since the application of the same approach to $\mathcal{G}_+$ should be straightforward. At long times and large lengths, the derivation should also hold for slanted coupling, with the replacement of $K/\sqrt{2}$ by K (see section 3).

In the imaginary-time path-integral representation, the Green's function $\mathcal{G}_-(\boldsymbol{r}_1, \boldsymbol{r}_2) \equiv \langle I_-(\boldsymbol{r}_1) I_-(\boldsymbol{r}_2)\rangle$ can read

$$\mathcal{G}_-(\boldsymbol{r}_1, \boldsymbol{r}_2) = \frac{1}{2K^2 Z} \prod_{\ell;\boldsymbol{r}} \sum_{n(\ell;\boldsymbol{r})} \int_0^{2\pi} \mathrm{d}\phi(\ell;\boldsymbol{r}) \left\{ \frac{\partial}{\partial\, \nabla_x \phi(1;\boldsymbol{r}_1)} - \frac{\partial}{\partial\, \nabla_x \phi(2;\boldsymbol{r}_1)} \right\} \times \left\{ \frac{\partial}{\partial\, \nabla_x \phi(1;\boldsymbol{r}_2)} - \frac{\partial}{\partial\, \nabla_x \phi(2;\boldsymbol{r}_2)} \right\} \exp\{-\mathcal{S}[n,\phi]\} \tag{A.1}$$

where the Euclidean action $\mathcal{S}$ is given by equation (11). By changing the variables from $\phi(\ell;\boldsymbol{r})$ and $\boldsymbol{m}(\ell;\boldsymbol{r})$ to $\phi^{\pm}(\boldsymbol{r})$ and $\boldsymbol{m}^{\pm}(\boldsymbol{r})$, respectively, one obtains

$$\mathcal{G}_-(\boldsymbol{r}_1, \boldsymbol{r}_2) = \frac{2}{K^2 Z} \prod_{\alpha=\pm} \prod_{\boldsymbol{r}} \sum_{\boldsymbol{m}^\alpha(\boldsymbol{r})} \int \mathrm{d}\phi^\alpha(\boldsymbol{r}) \, \frac{\partial}{\partial\, \nabla_x \phi^-(\boldsymbol{r}_1)} \, \frac{\partial}{\partial\, \nabla_x \phi^-(\boldsymbol{r}_2)} \exp\{-\mathcal{S}^+ - \mathcal{S}^-\} \tag{A.2}$$

where $\mathcal{S}^{\pm}$ have been given in equation (14). The $\phi^{\pm}$-integration can be performed easily by first introducing an auxiliary field as follows:

$$\mathcal{G}_-(\boldsymbol{r}_1, \boldsymbol{r}_2) = -\frac{2}{K^2 Z} \prod_{\alpha;\boldsymbol{r}} \sum_{\boldsymbol{m}^\alpha(\boldsymbol{r})} \int \mathrm{d}\phi^\alpha(\boldsymbol{r}) \int \mathrm{d}^2 \boldsymbol{J}^\alpha(\boldsymbol{r}) \; J_x^-(\boldsymbol{r}_1) J_x^-(\boldsymbol{r}_2) \exp\{-\mathcal{S}^+ - \mathcal{S}^-\} \tag{A.3}$$

where

$$\mathcal{S}^{\pm} = \frac{1}{\sqrt{2}K} \sum_{\boldsymbol{r},\boldsymbol{r}'} J_\tau^{\pm}(\boldsymbol{r}) \left[C^{\pm}(\boldsymbol{r},\boldsymbol{r}')\right]^{-1} J_\tau^{\pm}(\boldsymbol{r}') + \frac{1}{\sqrt{2}K} \sum_{\boldsymbol{r},\boldsymbol{r}'} \left[J_x^{\pm}(\boldsymbol{r})\right]^2 + \mathrm{i} \sum_{\boldsymbol{r}} \boldsymbol{J}(\boldsymbol{r}) \cdot \left[\boldsymbol{\nabla}\phi^{\pm}(\boldsymbol{r}) - 2\pi \boldsymbol{m}^{\pm}(\boldsymbol{r})\right]. \tag{A.4}$$

Integrating out $\phi^{\pm}(\boldsymbol{r})$, one finally gets the vortex representation of the Green's function $\mathcal{G}_-$:

$$\mathcal{G}_-(\boldsymbol{r}_1, \boldsymbol{r}_2) = \nabla_{\tau_1} \nabla_{\tau_2} \left\{ -\frac{\sqrt{2}}{K} U^-(\boldsymbol{r}_1, \boldsymbol{r}_2) + 4\pi^2 \sum_{\boldsymbol{r}_1', \boldsymbol{r}_2'} U^-(\boldsymbol{r}_1, \boldsymbol{r}_1') U^-(\boldsymbol{r}_2, \boldsymbol{r}_2') \left\langle v^-(\boldsymbol{r}_1') v^-(\boldsymbol{r}_2') \right\rangle_V \right\} \tag{A.5}$$

where the average $\langle \cdots \rangle_V$ is taken with respect to the total vortex Hamiltonian $H_V = H_V^+ + H_V^-$.

References

[1] Grabert H and Devoret M (ed) 1992 *Single Charge Tunneling: Coulomb Blockade Phenomena in Nanostructures* (New York: Plenum)

Averin D V and Likharev K K 1991 *Mesoscopic Phenomena in Solids* ed B L Al'tshuler, P A Lee and R A Webb (Amsterdam: Elsvier Science) p 167
Schön G and Zaikin A D 1990 *Phys. Rep.* **198** 237
[2] Averin D V, Korotkov A N and Nazarov Y V 1991 *Phys. Rev. Lett.* **66** 2818
[3] Matters M, Versluys J J and Mooij J E 1997 *Phys. Rev. Lett.* **78** 2469
[4] Delsing P, Haviland D B and Davidsson P 1996 *Czech. J. Phys.* **46** 2359
[5] Bradley R M and Doniach S 1984 *Phys. Rev.* B **30** 1138
[6] Fazio R and Schön G 1991 *Phys. Rev.* B **43** 5307
van Otterlo A, Wagenblast K-H, Fazio R and Schön G 1993 *Phys. Rev.* B **48** 3316
[7] Kim B J and Choi M Y 1995 *Phys. Rev.* B **52** 3624
Kim B J and Choi M Y 1997 *Phys. Rev.* B **56** 395
[8] Choi M-S, Yi J, Choi M Y, Choi J and Lee S-I 1998 *Phys. Rev.* B **57** R716
[9] Choi M-S, Choi M Y, Choi T and Lee S-I 1998 *Phys. Rev. Lett.* **81** 4240
[10] Berezinskii V L 1970 *Zh. Eksp. Teor. Fiz.* **59** 907 (Engl. Transl. 1971 *Sov. Phys.–JETP* **32** 493)
Kosterlitz J M and Thouless D J 1973 *J. Phys. C: Solid State Phys.* **6** 1181
[11] Kosterlitz J M 1974 *J. Phys. C: Solid State Phys.* **7** 1047
[12] See, e.g.,
Granato E 1990 *Phys. Rev.* B **42** 4797
Granato E 1992 *Phys. Rev.* B **45** 2557
Granato E 1993 *Phys. Rev.* B **48** 7727
[13] The critical behaviour of the system should not be affected by the choice of $\delta\tau$. See, e.g.,
Sondhi S L, Girvin S M, Carini J P and Shahar D 1997 *Rev. Mod. Phys.* **69** 315
Here, all the dynamics of the system occurs over the timescale ω_p^{-1}, making it appropriate to choose $\delta\tau \sim \omega_p^{-1}$.
[14] José J V, Kadanoff L P, Kirkpatrick S and Nelson D R 1977 *Phys. Rev.* B **16** 1217
[15] Korshunov S E 1990 *Europhys. Lett.* **11** 757
[16] See, e.g.,
Schön G and Zaikin A D 1990 *Phys. Rep.* **198** 237 and references therein